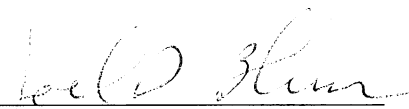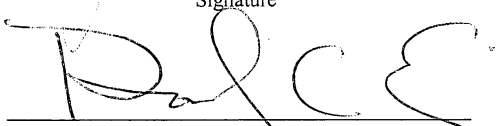Kelsey P. Johnson

Investigation of the deposition and emission of mercury in Arctic snow during an atmospheric mercury depletion event

Submitted for publication in: Journal of Geophysical Research - Atmospheres

in lieu of thesis in partial fulfillment
of the requirements for the degree of
Master of Science in Geology
Department of Geological Sciences
The University of Michigan

Accepted by:

Signature	JOEL D BLUM _Name_	2/1/08 _Date_
Signature	Rodney Ewing _Name_	4/11/08 _Date_
Department Chair	Rebecca Lange _Name_	4/14/08 _Date_

Investigation of the Deposition and Emission of Mercury in Arctic Snow During an Atmospheric Mercury Depletion Event

by

Kelsey P. Johnson

Coauthors:
    Joel D. Blum
    Gerald J. Keeler
    Thomas A. Douglas

TABLE OF CONTENTS

ACKNOWLEDGEMENTS

LIST OF FIGURES

LIST OF TABLES

ABSTRACT

Investigation of the Deposition and Emission of Mercury in Arctic Snow During an Atmospheric Mercury Depletion Event

by

Kelsey P. Johnson

Coauthors:
    Joel D. Blum
    Gerald J. Keeler
    Thomas A. Douglas

Mechanisms of air-snow exchange of mercury (Hg) during and after atmospheric mercury depletion events (AMDE) remain poorly constrained and limit our understanding of the Arctic Hg cycle. In an intensive field study we measured the Hg concentrations of surface snow through time and carried out flux chamber emission experiments during AMDE and non-AMDE conditions in the spring of 2006 near Barrow, Alaska. Clear skies, low wind speed, on-shore winds and a stable boundary layer characterized the meteorology during AMDE conditions. Surface snow Hg concentrations increased throughout a nine-day AMDE from background levels (4.1 to 15.5 pg/g) to elevated levels (147 and 237 pg/g) at both sampling sites and returned to near-baseline values within two days of return to non-AMDE conditions. The Hg concentrations of core samples from the full snowpack did not increase significantly during the AMDE and demonstrate that the deposition of atmospheric Hg is mostly to surface snow during AMDEs. Complete oxidation and deposition of background gaseous elemental Hg in the near-surface troposphere to a height of 150-450 m can account for the Hg gains observed in the surface snow. Snow incubated in field-based flux chambers

emitted 4 to 7% of its total Hg content within one day. This emission rate may represent an upper limit for the photo-reduction rate of "easily" reducible Hg in snow during natural conditions. Late springtime full-column snow core samples have low Hg concentrations which implies that the majority of the Hg deposited during AMDEs was a transient surface phenomenon at this location.

INTRODUCTION

Projected changes in the Earth's climate may alter global contaminant transport pathways [*Macdonald, et al.,* 2005] and may enhance mercury (Hg) deposition to high latitude ecosystems by changing the nature, amount and timing of precipitation [*Lindberg, et al.,* 2002]. Following deposition to terrestrial ecosystems from the atmosphere, Hg can be transformed into its more toxic form, methylmercury, which strongly biomagnifies in aquatic food webs and presents a major source of human exposure to Hg [*Magos and Clarkson,* 2006]. This provides a potential transport pathway to humans in coastal populations reliant upon fish and piscivorous mammals for subsistence [*Wheatley and Paradis,* 1995].

The biogeochemical cycle of Hg is complex (see review by Fitzgerald and Lamborg, [2003]) because Hg has two environmentally active redox states including a mobile, monatomic gas phase (Hg^0). Hg^0 is well mixed globally with an atmospheric lifetime of about 1 year [*Schroeder, et al.,* 1998; *Slemr, et al.,* 1985] which enables long-range atmospheric transport to remote locations and results in an atmospheric background concentration of 1.3 to 1.7 ng/m^3 [*Ebinghaus, et al.,* 2002; *Slemr, et al.,* 2003]. However, this lifetime estimate was recently challenged due to new insights into the atmospheric chemistry of Hg, and these studies suggest the lifetime of Hg will likely be much shorter [*Landis, et al.,* 2005]. Reactive gaseous mercury (RGM, Hg^{2+}) and particulate mercury (Hg_P) are procedurally defined atmospheric Hg species [*Landis, et al.,* 2002] with shorter atmospheric lifetimes and variable background concentrations typically orders of magnitude less than Hg^0.

Both ozone and GEM depletions are chemical phenomena associated with polar sunrise. Tropospheric ozone depletion events were first reported in Barrow, Alaska in 1986 [*Oltmans and Komhyr,* 1986] and atmospheric mercury depletion events (AMDEs) were first observed at Alert, Canada in 1995 [*Schroeder, et al.,* 1998]. During tropospheric ozone depletion events, O_3 mixing ratios drop from background values of 25 to 35 ppb(v) to nearly 0 ppb(v). AMDEs occur seasonally in high-latitude, coastal regions during the interval between polar sunrise and spring snowmelt. During AMDEs, Hg^0 concentrations drop well below 1 ng/m^3 for periods of hours to days concurrently with ozone depletions. Numerous studies have documented AMDEs in the Arctic [*Berg, et al.,* 2003; *Ferrari, et al.,* 2005; *Gauchard, et al.,* 2005; *Lu, et al.,* 2001; *Schroeder, et al.,* 1998; *Steffen, et al.,* 2003; *Steffen, et al.,* 2005], the Antarctic [*Ebinghaus, et al.,* 2002; *Sprovieri, et al.,* 2005] and the sub-Arctic [*Kirk, et al.,* 2006; review by *Steffen, et al.,* 2007]. Ozone molecules are catalytically destroyed and atmospheric Hg^0 atoms are oxidized during AMDEs. Similar to stratospheric ozone depletion, AMDEs result from photochemical reactions involving halogen oxidants and heterogeneous reaction sites on ice crystals (see review by Barrie and Platt [1997]). Unlike stratospheric ozone depletion, atomic Br rather than Cl is thought to be the dominant halogen destroying tropospheric O_3 and oxidizing Hg^0 during AMDEs [*Barrie, et al.,* 1988; *Simpson, et al.,* 2005 and references therein]. Photolabile Br molecules are wicked to the atmosphere through brine channels that form in sea ice of refreezing sea water [*Simpson, et al.,* 2007]. Goodsite and others [2004] propose that the following exothermic reactions lead to tropospheric Hg^0 oxidation:

Hg + Br (+ M) $\leftrightarrow$ HgBr   (M = third body)

HgBr + Y (+ M) $\rightarrow$ HgBrY   (Y = Br, I, OH, O_2, etc.)

Mercury concentrations in Arctic surface snow have been observed to increase dramatically during AMDEs [*Lindberg, et al.,* 2002] and to become increasingly bio-available during snowmelt [*Scott,* 2001]. As much as 90% of a snowpack Hg content may enter the melt water reservoir upon snowmelt [*Dommergue, et al.,* 2003]. Kinetic modeling studies estimate gross AMDE inputs of Hg to the Arctic of 100 tons/year [*Ariya, et al.,* 2004] and 119 tons/year [*Skov, et al.,* 2004]. However, more detailed studies reveal that Hg concentrations in snow vary temporally and spatially [*Douglas, et al.,* 2005] and this variability is a function of snow provenance [*Douglas, et al.,* in press]. Therefore, mass balance models do not adequately consider Hg loss from the snowpack by (photo)reduction and subsequent emission. Annual emission estimates of Hg from snow in Arctic regions vary widely and suggest that our understanding of the Arctic Hg cycle and net ecosystem loading is highly uncertain.

The objective of this study is to better constrain mechanisms of air-snow Hg exchange during and after AMDE conditions. We used high temporal resolution snow and air sampling to monitor Hg gain and loss from seasonal snow at an Arctic coastal location near Barrow, Alaska [71.32°N, 156.6°W] during a single AMDE. Barrow is distant from major pollution point sources and is known to experience AMDEs [*Brooks, et al.,* 2006; *Lindberg, et al.,* 2001; *Lindberg, et al.,* 2002]. Our intensive field study spanned March 13 - April 4, 2006, with additional samples collected throughout the spring and during snowmelt. Mercury concentrations from a suite of surface snow samples are reported in a time-series from two locations before, during and after a

mercury depletion event. We know of no other surface snow time-series of this resolution and duration. Flux chamber experiments were designed to quantify Hg emission under closely monitored conditions. Several experiments were performed and ranged from those very similar to natural snowpack conditions to those with variable temperature, UV intensity or initial snow Hg concentration.

Sample bottle and flux chamber cleaning procedures

Snow samples were collected in FEP Teflon bottles extensively cleaned by the following procedure. Bottles were first rinsed with acetone, washed in warm water with Citrinox soap, rinsed five times with water purified by reverse osmosis and soaked in a hot 3.5% HNO_3 bath for six hours. In a clean room, bottles were rinsed 5 times with 18.2 $M\Omega$ deionized water (DIW) and filled with 1% BrCl for at least 12 hours. Bottles received five final rinses with DIW and blank Hg values measured on >10% of the bottles yielded less than 6 pg of Hg per 25 mL of blank solution. Flux chambers were washed with 5% HCl and were dried and bagged in a clean room prior to shipment to the field site. A polyethylene shovel used to fill chambers with surface snow was washed in 10% HCl in a laboratory prior to its use and was rinsed with DIW in a field laboratory between sample collections. PVC tubing was rinsed with DIW before being used to collect snowpack cores.

Snow sampling procedures and study site

Three types of snow samples were collected in this study and their Hg concentrations are referred to as $Hg_{surface}$, Hg_{core}, and $Hg_{snowfall}$. Surface samples were collected from the upper 1 cm of the snow surface and represent recently blowing snow or stagnant surface snow ($Hg_{surface}$). Core samples were collected periodically from the entire snow column and represent composites of two to four cores collected with a 5 cm diameter PVC pipe and mixed into one large FEP Teflon container (Hg_{core}). Snowfall

samples were collected in Pyrex trays elevated on a rack 1.5 meters above the snow pack surface. Saltating snow grains rarely get above 0.5m during wind transport [*Pomeroy and Gray,* 1990] and therefore collect represent precipitation and/or condensation rime ($Hg_{snowfall}$).

Care was taken to approach sampling locations from the downwind direction to prevent contamination. Either a polystyrene scoop washed in 10% HCl or the lip of an acid-cleaned Teflon bottle was used to transfer snow into collection bottles. All samples remained frozen, sealed with Teflon tape and triple bagged in lock-seal plastic bags during shipment to the University of Michigan for chemical analysis.

Site 1 is on a low relief, gently rolling landscape typical of the region and is located 7 km northwest of Barrow and 2.5 km southeast of the coast. Sampling occurred each morning between 08:45 and 17:00 Alaska Standard Time (GMT -9 hours; AST), and samples were collected during the narrower time period of 08:45 and 09:40 AST from March 23 through March 31. Surface samples were collected daily between March 13 to April 2 and on April 27, May 20 and May 31. Snow cores were collected four times during the intensive study on March 23, 26, 29 and April 1 and later in the spring season on April 27 and May 31. Snowfall samples were collected each day that new snow was present in the elevated collection trays: March 15, 16, 19, 20, 21, 22, 25 and April 1 and 2.

Site 2 was a snow drift on the leeward side of a fence located 7 km northwest of Barrow and 1.3 km southeast of the coast. Surface snow sampling occurred each morning prior to exposure to direct sunlight between 7:25 and 10:40 AST and after exposure to roughly 12 hours of sunlight between 20:15 and 22:10 AST each evening.

Surface snow used to fill flux chambers (described below) was collected at this location during morning sampling.

Flux chamber experiments

Several flux chamber experiments were performed and are summarized in Table 1. Chambers were filled with snow to a height of 8-12 cm and weighed before being bagged, covered with an opaque outer bag, transported on foot to an outdoor incubation location at the Barrow Arctic Science Consortium (BASC) and installed within 1 hour. The chambers were designed to simulate natural chemical conditions by allowing unfiltered, ambient air containing photo-labile oxidants such as Br_2, H_2O_2, and O_3 to enter the chamber through an inlet tube (Figure 1). The chamber inlet was an unheated, 50 cm long Teflon tube (0.64 mm outer diameter) designed to capture incoming Hg^{2+} by sorption to its walls. The inlet tubing was sheathed by an opaque plastic outer tube to prevent photochemical re-mobilization of Hg^{2+} sorbed to the inner tube. Flux chambers consisted of 40 L translucent polypropylene, rectangular bins. A flat piece of 1.27 cm thick polycarbonate served as the removable chamber lid and had two 28 cm x 30.5 cm holes removed as windows. The inner surface of the lid was lined with 5 mil PFA Teflon film to allow full-spectrum light transmittance through the windows.
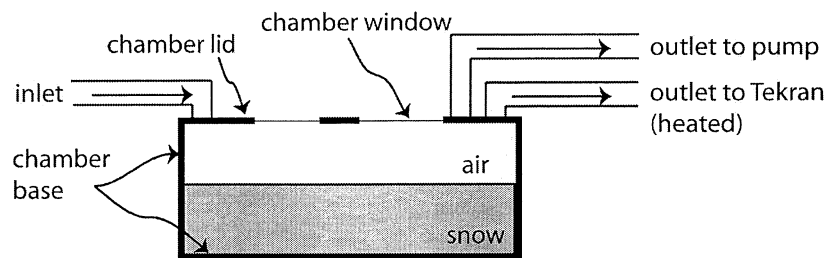
Figure 1: Flux chamber design. The chamber lid was composed of ¼" polycarbonate frame with 28 x 30.5 cm windows cut in it. A 5 mil PFA Teflon film covered the inside of the chamber lid. Clamps and a gasket sealed the chamber lid to the chamber base. Four ¼" holes were threaded into the frame to support compression fittings, which sealed inlet and outlet Teflon tubing.

Experiment 1 measured a procedural chamber blank, which exceeded ambient atmospheric Hg values by less that 1 ng TGM/m^3 (Figure 8a). Contamination by the chamber materials was therefore insignificant compared to concentrations observed during incubation experiments. Snow used in Experiment 2 was collected two days before exposure in the flux chamber from a snowpack overlying sea ice. Surface snow was shoveled into a double-bagged polyethylene bag, transported to the research station, homogenized and transferred into a flux chamber base. Experiments 3, 4, 5 and 6 utilized snow collected from Site 2 under ambient light, temperature and $Hg_{surface}$ conditions. Snow was shoveled directly from the collection site into flux chambers to minimize compaction, disturbance and sintering in Experiments 3, 4, 5, 6 and 7. Visible alteration of the snow structure by warming or compression during this preparation was negligible. Experiment 7 operated two identical chambers, one of which received UV-attenuated radiation (7a) while the other received ambient solar radiation (7b). After one day of incubation, chamber 7a was opened and 9.8 g of a 170 ng/g Hg standard solution was applied as a fine mist. This snow was homogenized, sub-sampled to determine the Hg concentration and re-installed as Experiment 8. Snow in experiment 8, therefore, underwent some structural metamorphism due to stirring.

Air from each chamber's headspace (10-20 L) was sampled continuously at a rate of 2.5 L/min. Headspace air was withdrawn through one outlet at a rate of 1.5 L/min at STP and into a Tekran 2537A Hg analyzer (described below) through Teflon tubing insulated and heated to 50-60°C to prevent Hg loss by sorption to tubing walls. Air was withdrawn from a second chamber outlet at a rate of 1.0 L/min by a pump to increase the chamber's flushing rate. A Tekran Model 1110 Synchronized Two Port Sampling System was used to alternate total gaseous mercury (TGM) measurements between flux chambers and either procedural blanks or ambient air every third measurement (i.e. every ten minutes). Consecutive measurements were averaged to yield a single data point every 10 minutes that alternated between chamber outlet (C_{out}) and procedural blank or ambient (C_{in}).

The starting times and duration of the flux chamber experiments varied somewhat due to difficult field logistics. To allow comparison between experiments, we compared chamber emissions during the three-hour interval of peak emission between 12:30 – 15:30 (abbreviated as "mid-day TGM fluxes"). The mid-point between consecutive blanks (C_{in}) was interpolated and subtracted from the matching chamber time-step (C_{out}). Mid-day fluxes (F) were calculated by summing the difference between C_{out} and B over the three hour interval, multiplying by the total flow rate (Q = 2.5 L/min) and a unit conversion factor (k = 20 minutes*m^3/1000 L) and dividing by the surface area of snow within the chamber (A = 0.28 m^2). Midday emission fluxes, in ng Hg/m^2/hr, represent the average TGM emission during the three hour interval from 12:30 to 15:30:

$F = 1/3* \sum_{12:30-15:30} (C_{out} - C_{in})*Q*k/A$

Total daily (E_{total}) and mid-day Hg emissions (E_{midday}) were calculated for each experiment by:

$$E_{total} = \Sigma_{experiment\ interval}\ (C_{out} - C_{in})*Q*k$$

and

$$E_{mid\text{-}day} = \Sigma_{12:30\text{-}15:30}\ (C_{out} - C_{in})*Q*k.$$

Analytical techniques

TGM was monitored in ambient air and from flux chambers using two Tekran model 2537A Cold-Vapor Atomic Fluorescence Spectrometers (CVAFS). The CVAFS operates two parallel gold traps which sample TGM continuously and measure Hg concentrations at five minute intervals. Mercury concentration in snow was quantified using a Nippon Instruments MA 2000 Atomic Absorption Spectrometer (AAS). Samples were acidified with BrCl in a clean room during thawing to 1 vol.% BrCl to preserve total Hg as Hg^{2+} in solution. BrCl was neutralized with 20 μL concentrated hydroxylamine and aqueous Hg^{2+} was chemically reduced with 250 μL each of 50% H_2SO_4 and 10% $SnCl_2$ prepared according to EPA Method 1631e. Reduced Hg^0 was purged from the sample solution, pre-concentrated on an in-line gold trap and thermally desorbed into the AAS detector by heating to 650°C. NIST 3133 Hg standard was used to cross-check the accuracy of the Nippon Instruments calibration standard. The limit of quantification of 1.0 pg/g is defined as 3SD of blanks run within analytical sessions. Replicate analyses of 100 pg/g standards yielded a 1SD analytical uncertainty of $\pm$ 2.5 pg/g. Duplicate analyses were performed on over half the samples and reproduced within 10%. Samples with concentrations less than 10 pg/g had a 1SD uncertainty of $\pm$ 1 pg/g. The relative

standard deviation of field replicates collected for twenty-one snow samples ranged from 0 to 46% and had a mean relative standard deviation of 10%.

Ozone was measured in ambient air using a TEI 49C UV photometric gas analyzer that sampled from an elevation of 2 m above the snow surface. In addition, hourly averages of ozone concentration were obtained from the NOAA Climate Monitoring and Diagnostic Laboratory Barrow Observatory (CMDL) located 8 km east of Barrow and 2 km from our study site at BASC at an elevation of 3 m.

Ancillary data include meteorological data and satellite images of the coastal sea ice. Hourly wind speed and direction data were obtained from CMDL for the duration of the study. Moderate Resolution Imaging Spectroradiometer (MODIS) images were obtained from the University of Colorado and provide insight to the location and morphology of sea-ice fractures and leads off the Arctic Ocean Coast near Barrow. Temperature of ambient air and air within flux chambers was recorded at 4 or 5 minute intervals using four temperature sensors (Onset Inc. HOBO Temperature Data Loggers). Diffuse light intensity was measured with three Onset Inc. HOBO Light Intensity Data Loggers (detection range: 0.01 to 10,000 lumens/ft^2; centered on 555 nm). One datalogger was covered with 5 mil PFA Teflon film to simulate diffuse light penetration through the chamber windows.

RESULTS

Ozone mixing ratios and meteorological conditions

Surface ozone measurements from CMDL during our study are presented in

Figure 2 and strongly correlate with ozone data measured at our study site ($r^2 = 0.96$;

Figure 2 inset). AMDE conditions are defined in this study as periods when hourly

averages of CMDL ozone mixing ratios fell below 15 ppb(v). Therefore, AMDE

conditions occurred continuously for nine-days from pre-dawn on March 22 to near

midnight on March 30, 2006 at Barrow, Alaska.
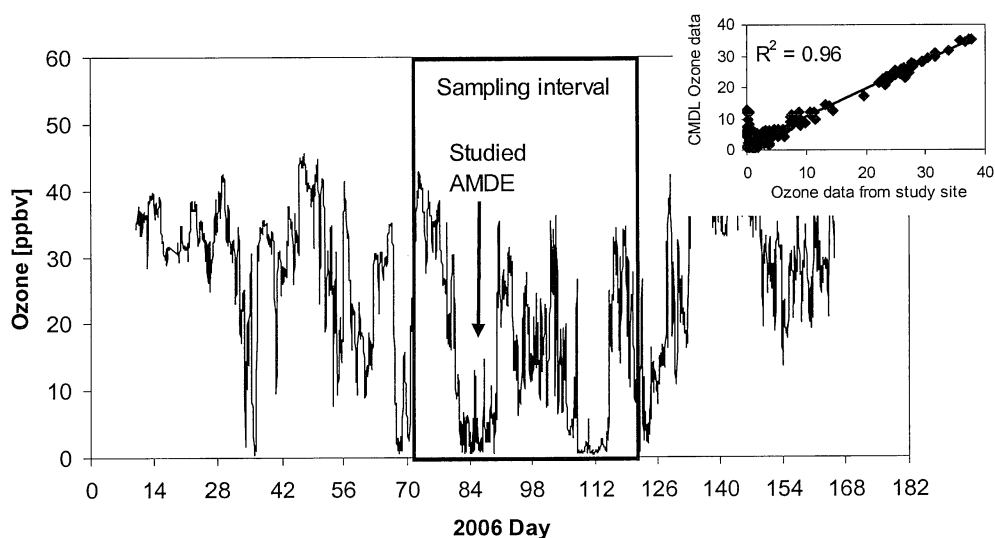
Figure 2: CMDL hourly ozone data from ambient air during the 2006 AMDE season. Inset shows the strong correlation between CMDL concentrations and those made at our study site 2 km away.

Wind speed and direction varied bimodally between strong, continental winds

during normal non-AMDE conditions, and weak coastal winds during AMDE conditions

(Figure 3). Winds during AMDEs therefore passed over marine halogen sources that

include newly formed sea ice and/or sea water exposed in open ice leads. During non-

AMDE conditions, easterly winds averaged 7.8 ± 2.9 m/s (1 SD) (range = 0.3 - 13.7 m/s)

12

and are associated with blowing snow events and the shearing of sea ice to create fractures (leads) in the sea ice north and west of Barrow (Figure 4). Leads were present from March 11 to 21 and again after March 30th. During AMDE conditions, westerly winds averaged 2.0 ± 1.1 m/s (1 SD) (range: 0 to 5.2 m/s) and mobilization of snow by wind was not observed. For example, footprints made during sample collection remained intact throughout the AMDE, whereas footprints during non-AMDE conditions were filled with saltating snow grains, scoured and/or re-worked within minutes.
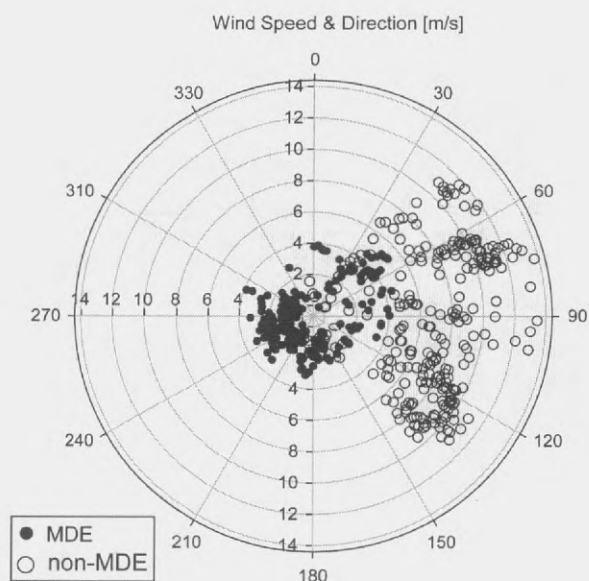
Figure 3: Wind speed (m/s) and direction during normal and AMDE conditions as defined by pO_3. Non-AMDE conditions span 3/13/06 0:00 - 3/21/06 7:00 and 3/31/06 15:00 - 4/3/06 23:00 when $pO_3 > 15$ ppb(v). AMDE conditions span 3/22/06 03:00 - 3/30/06 23:00 when $pO_3 < 15$ ppb(v).
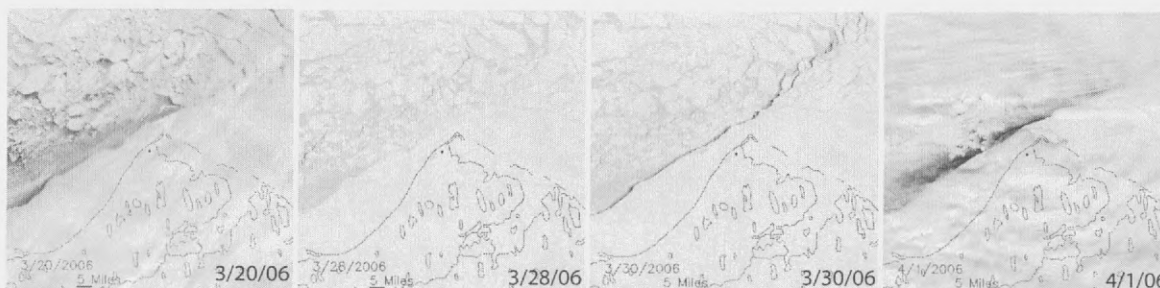
Figure 4: MODIS satellite images (courtesy of U. Colorado) of the sea and land fast ice (white), exposed ocean water (dark) and land (outlined). The ocean is exposed preferentially during non-AMDE conditions; clouds obscure view, especially on 4/1/06.

Hg concentrations in surface snow

Significant increases in surface snow Hg concentrations occurred during AMDE conditions at both sampling sites. At Site 1, $Hg_{surface}$ increased step-wise from background concentrations during non-AMDE conditions to elevated concentrations within three days of the AMDE onset (Figure 5a). Specifically, $Hg_{surface}$ at Site 1 increased from 10 pg/g (March 13) to a concentration plateau of 194 ± 22 pg/g (23-30 March) and then dropped to 53 pg/g (2 April) within 2 days of AMDE cessation. Assuming a snow density of 0.20 to 0.34 g/cm^3 [*Sturm and Liston,* 2003], we observed between 370 and 640 ng/m^2 Hg was deposited to the upper 1 cm of the snowpack at Site 1 during the observed AMDE.

In contrast, $Hg_{surface}$ at Site 2 increased gradually from 35 pg/g (22 March) to a peak of 147 pg/g (29 March), with an average increase of 16 pg/g per day (Figure 5b). Note that sample collection at Site 2 began during the first day of AMDE conditions and $Hg_{surface}$ was already elevated above background. A diurnal pattern in $Hg_{surface}$ is evident from "morning" and "evening" samples in which the Hg concentration increased overnight and either decreased or remained constant during the daytime (Figure 5b). Following the same assumptions as for Site 1, we estimate surface snow at Site 2 gained 220 to 380 ng/m^2 Hg during this AMDE. Surface hoar (large feathery crystals that coat horizontal and vertical surfaces after intense radiation cooling; [*Colbeck,* 1988]) was present on all snow surfaces surrounding Site 2 during the AMDE and may facilitate a different Hg^{2+} scavenging mechanism than at Site 1 [*Douglas, et al.,* in press]. Surface hoar crystals grew from initial lengths of < 0.5 cm (22 March) to over 3 cm by the end of the AMDE (31 March, morning only) and were also observed along pressure ridges in the

sea ice. Four field replicates of surface hoar coating various faces of a pressure ridge ice boulder contained 99 ± 13 pg/g (2SD) on 29 March. After AMDE conditions ended, surface hoar crystals were quickly destroyed by wind erosion and Hg$_{surface}$ diminished to near-initial levels within two days (41 pg/g on 2 April).

Freshly fallen snow and ice crystals contained the highest Hg concentrations observed in this study and previous studies at this location [*Douglas, et al.,* in press]. Values of Hg$_{snowfall}$ averaged 485 ± 385 pg/g (n=9) and ranged from 20.8 (21 March) to 1120 pg/g (16 March) (Figure 6). The highest snowfall concentrations (> 400 pg/g) were observed during non-AMDE conditions and lower concentrations (i.e. < 100 pg/g) were observed during AMDE conditions, with the exception of one sample that contained 363 pg/g (25 March).
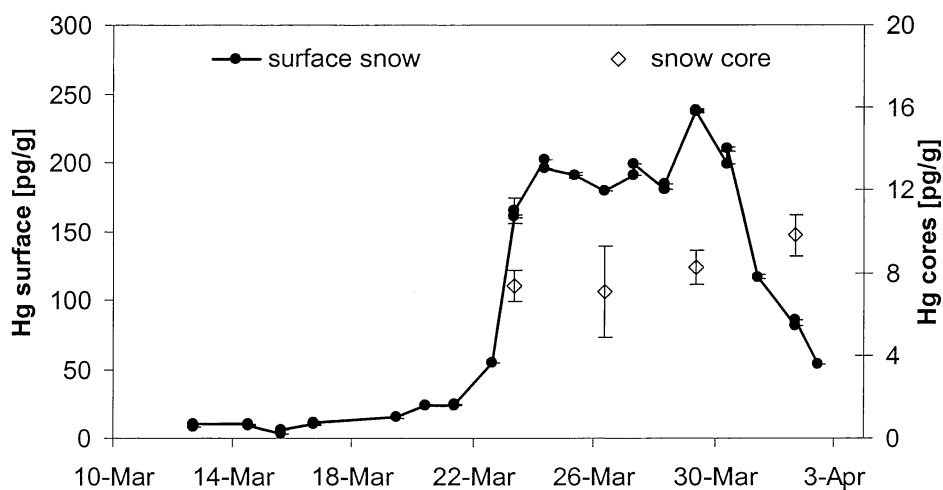
Figure 5a: Time-series of Hg$_{surface}$ at Site 1: Hg$_{surface}$ increases in surface snow during an AMDE. Four full-column depth cores were sampled during and after AMDE conditions and use the vertical scale on the right. Data points are larger than 1σ analytical precision except where indicated by error bars.
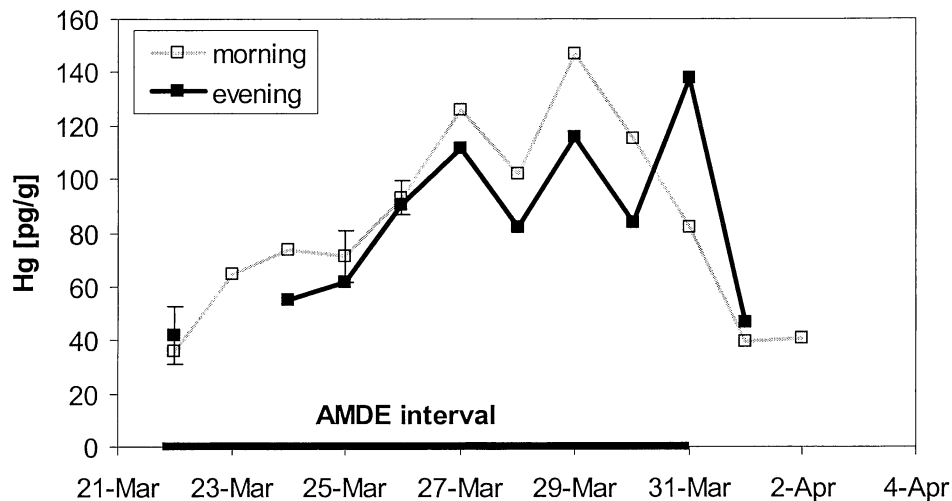
Figure 5b: Time-series of Hg$_{surface}$ at Site 2: Hg$_{surface}$ collected in the morning, after ~12 hours of darkness, and in the evening, after ~12 hours of daylight. Data points are larger than 1σ analytical precision; error bars indicate heterogeneity of replicate field samples. Horizontal bar demarcates AMDE interval.
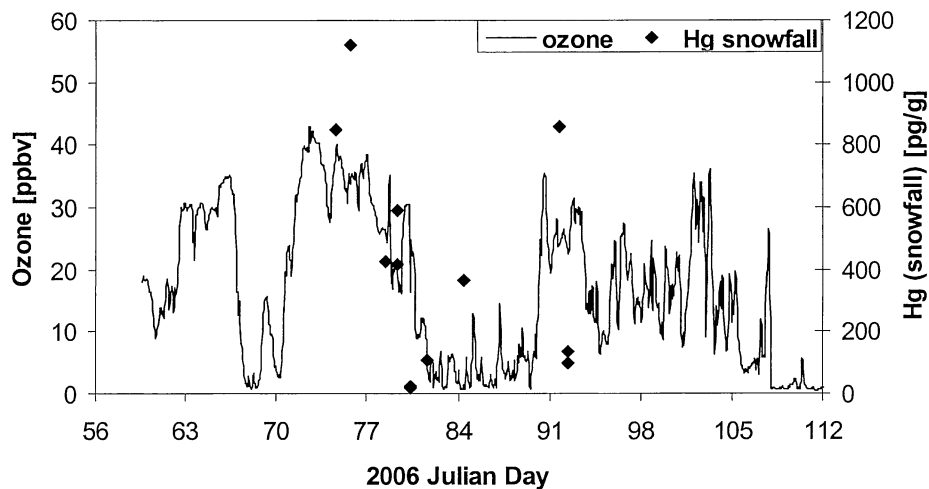
Figure 6: Time-series of diamond dust snowfall with respect to ambient pO_3 concentration. Note difference in vertical scales.

16

Snow cores and late spring samples

Full snowpack cores were collected from Site 1 during and after AMDE conditions to assess the total snowpack Hg content during and following AMDE conditions. The snowpack ranged in depth from 26 to 50 cm and contained 7.6 ± 0.6 (1SD) pg/g Hg during the AMDE (n=3) with no significant difference from a core collected after the return to normal, non-AMDE conditions (9.8 pg/g, n=1). Surface and core samples collected in late spring from Site 1 had decreasing Hg concentrations (Figure 7). Specifically, late springtime surface snow contained 45 pg/g (April 27), 10 pg/g (May 20) and 11 (May 31, upper 0.5 cm), while full-column snow cores contained 2.5 pg/g (33 cm), 2.2 pg/g (42 cm) and 5.1 pg/g (30 cm), respectively.
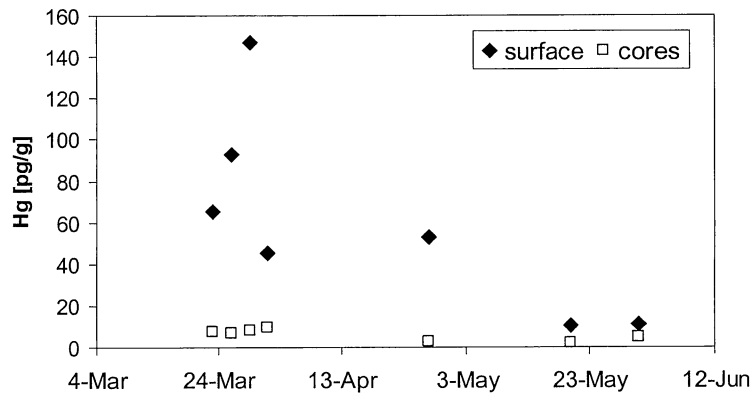
Figure 7: Mercury concentration (pg/g) of surface and snowpack cores from Site 1 throughout the AMDE and melt seasons. Melt occurred in late May.

Flux chamber experiments

Eight flux chamber experiments were performed to investigate TGM emission rates from natural Arctic snow under ambient temperature, ambient and UV attenuated radiation, and ambient and enhanced Hg concentrations. Specific procedures for each experiment are described above in Methods and summarized in Table 1. Figure 8 presents TGM emission and associated blanks for each experiment (note different vertical scales); Table 2 summarizes Hg emission and flux quantities. TGM emission profiles always peaked shortly after solar noon and dropped below detection during hours of darkness. Some profiles deviated from bell-shaped curves as a result of low signal to noise ratios (Exp 1), lids being briefly removed from the chamber and blank during operation (Exp 3), or temporarily clogging of the outlet tubing (Exp 6).

The total Hg content of snow initially within the flux chambers averaged 520 ng and ranged from 215 to 1520 ng. Flux chambers incubated under ambient conditions emitted an average of 20 ± 11 ng TGM/day (1 SD) and ranged from 8.0 to 39 ng TGM/day. Within the three-hour mid-day interval under ambient conditions, TGM emission averaged 9.3 ± 5.4 ng (1 SD) and ranged from 4.7 to 19 ng. The chamber experiment in which 1.1 µg of Hg was added as liquid mist emitted 68 ng TGM/day, 32 ng of which was emitted within the mid-day interval.

We measured the effects of heating the chamber and of the wavelength of incoming radiation on TGM emission using a heated flux chamber (data not shown) and a UV filter experiment (Figure 8, Exp 7). In the heating experiment, a flux chamber was heated above ambient temperatures (but still below -10°C) from 22:15 (30 March) through 11:40 the following morning. TGM emission was detectable beginning at

approximately 03:00 when it began rising gradually to 6.8 ng/m^3 at 08:40. At 08:40, the chamber was covered with opaque plastic and TGM emission rate stabilized at approximately 7 ng/m^3 for the remaining three hours of experimentation. Temperatures in all other experiments remained below -15°C due to very low ambient temperatures (range: -12 to -38°C) and neither melting nor snow grain metamorphism due to warming within the chambers was visually observed. Experiment 7 consisted of one of two parallel chambers being covered with a polycarbonate filter that completely attenuated UV radiation without attenuating visible light (~405 nm cut-off, Figure 9). As a result of the decrease in UV intensity, the TGM flux decreased by 25% and the TGM emission pattern showed no change (Figure 8, Exp7).

Transmittance properties of various chamber media used in our experiments are presented in Figure 9. The Teflon chamber window transmitted 65-71% of direct UV$_B$ (290-320 nm), 71-80% of direct UV$_A$ (320-400 nm), and 80-87% of direct visible light (400-700 nm) in laboratory tests, while a transmittance of diffuse light of 40% was measured in the field. Direct UV transmittance through the vertical chamber walls was a maximum of 40% during laboratory tests, and UV transmission through the walls was not measured in the field. We estimate that a maximum of 20% direct UV$_B$ and 30% direct UV$_A$ entered the chamber through its vertical walls during field experiments.

Table 1: Flux Chamber Experiment Descriptions

Experiment	Date	Time	Conditions	Description (collection date)
1	25-Mar	10:10 - 22:00	ambient	Ambient vs. chamber blank
2	22-Mar	8:05-21:10	ambient	Snow overlying sea ice (3/20). Underwent some compaction during transport.
3	23-Mar	10:45-21:10	ambient	Surface snow from Site 2 (3/23)
4	24-Mar	10:05-21:10	ambient	Surface snow from Site 2 (3/24)
5	27-Mar	10:40-21:10	ambient	Surface snow from Site 2 (3/27)
6	31-Mar	10:45-19:10	ambient	Surface snow from Site 2 (3/31), non-AMDE conditions
7	29-Mar	10:05-21:10	UV attenuated	Surface snow from Site 2 (3/29). Chamber 7a received UV-attenuated radiation Chamber 7b received ambient light
8	30-Mar	9:20-21:40	artificially high $Hg_{surface}$	Hg standard applied to snow used in Chamber 7a (3/29). $Hg_{surface}$ likely more heterogeneous than in other experiments

Table 2: Flux Chamber Results

		Experiment #							
Property	units	2	3	4	5	6	7a	7b	8
HgT, initial	pg/g	54.8	64.7	73.7	118	82.4	147	147	422
Total Hg in chamber, initial	ng	215	225	230	600	220	575	575	1520
Total Chamber Hg, final	ng	55.7	53.7	52.7		87.0	97.8	97.8	408
Hg exposed (1cm surfaces)	ng	77	90	103	164	115	82	206	590
Visible light intensity, mid-day average	L/sf/hr	713	744	965	811		1310	1310	1310
Mid-day Hg Emission									
mid-day emission	ng	4.7	6.5	7.4	19	3.5	10	14	32
mid-day hourly average	ng/hr	1.6	2.2	2.5	6.2	1.2	3.4	4.7	11
% emitted mid-day, exposed	%	7.3%	8.6%	8.6%	13.5%	3.6%		8.1%	6.4%
% of total Hg emitted per mid-day hr	%/hr	0.7%	1.0%	1.1%	1.0%	0.5%	0.6%	0.8%	0.7%
% of bulk Hg emitted at mid-day	%/mid-day	2.2%	2.9%	3.2%	3.1%	1.6%	1.8%	2.4%	2.1%
Daily Hg Emission									
daytime emission	ng/day	11.6	13.7	16.8	38.5	8.0	22.8	29.4	67.6
# intervals		40	32	34	32	26	34	34	35
% Hg emitted from exposed volume	%	15%	15%	16%	23%	6.9%	28%	14%	11%
% Hg emitted	%/day	5.4%	6.1%	7.3%	6.4%	3.6%	4.0%	5.1%	4.4%
% of daily emission at mid-day	5	41%	47%	44%	48%	44%	45%	48%	47%
Hg Flux									
hourly flux at mid-day	ng/m2/hr	5.6	7.7	8.9	22	4.2		17	38
daily flux	ng/m2/day	41	49	60	140	29	82	105	240
% of daily flux at mid-day	%	14%	16%	15%	16%	15%		16%	16%
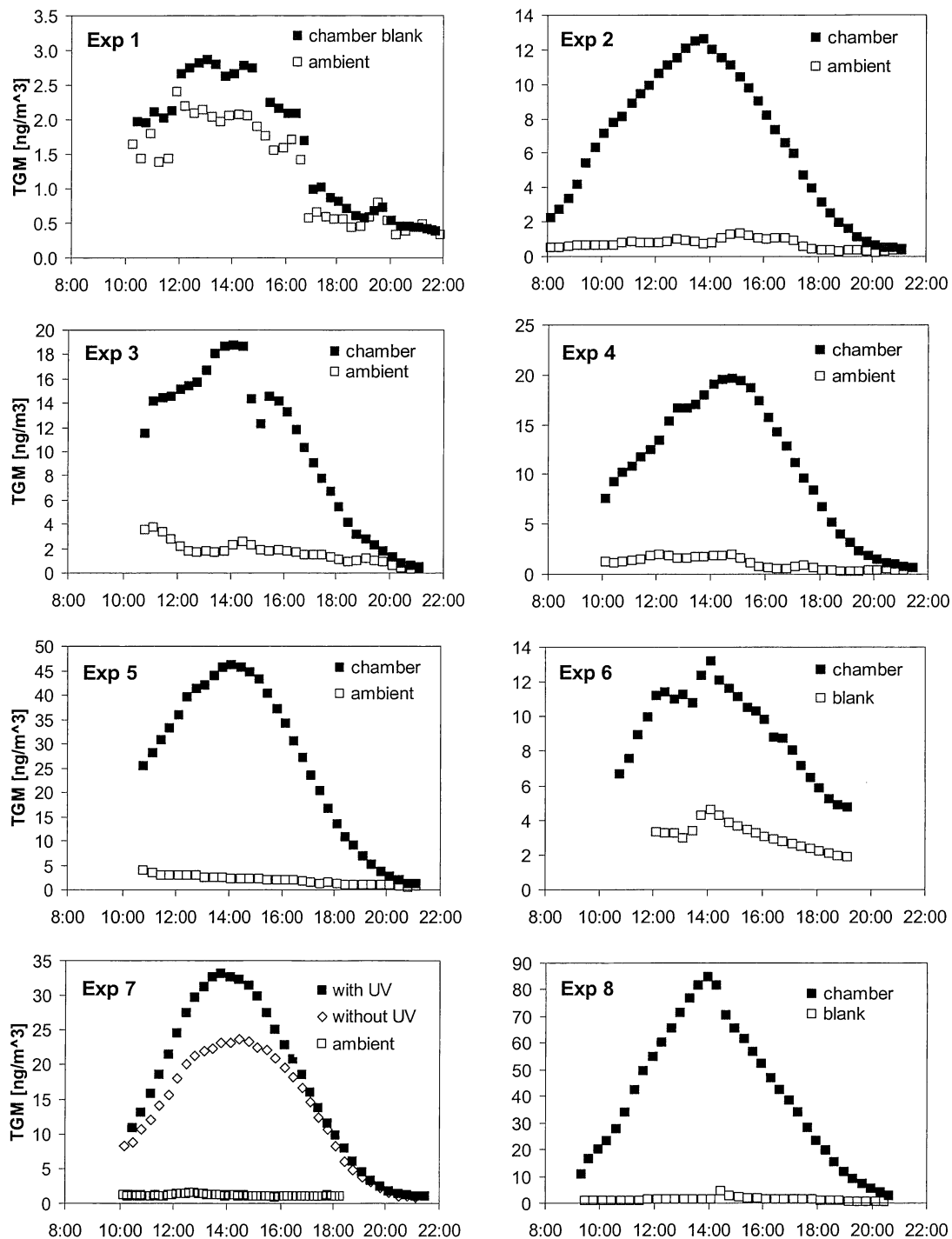
Figure 8: TGM emission profiles from eight chamber experiments. Exp 1 measured Hg concentration from a chamber blank compared to ambient air; Exp 2, 3, 4 and 5 operated during the AMDE under ambient conditions; Exp 6 operated during non-AMDE conditions; Exp 7 used two parallel chambers which received either UV-attenuated light (7a) or ambient light (7b); Exp 8 incubated snow with artificially enhanced Hg content and operated during transition to non-AMDE conditions. See Table 1 for details.
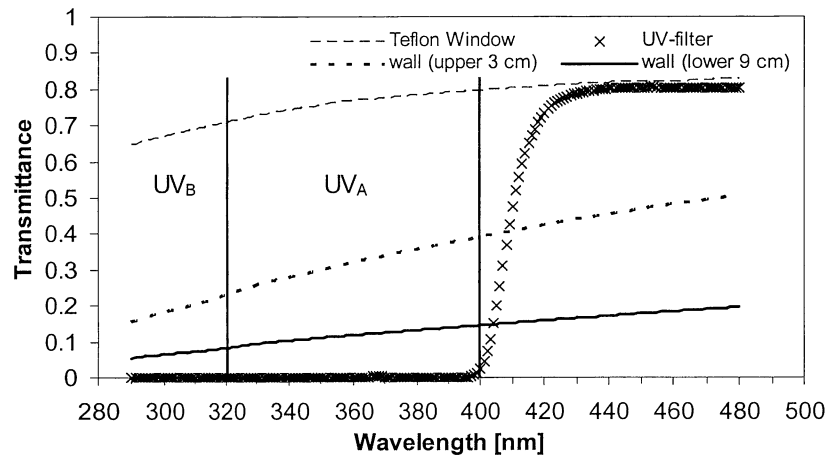
Figure 9: Transmittance properties of chamber materials.

DISCUSSION

Factors leading to atmospheric mercury depletion events

Meteorological and chemical data from this study are consistent with previous observations that AMDEs occur in coastal locations under conditions of low wind speed, a stable boundary layer (e.g. temperature inversion), sunlight, freezing temperatures and the availability of photolabile halogens [*Lu, et al.,* 2001]. During AMDE conditions, winds passed over re-freezing sea water before reaching the study site (22 to 31 March), transporting halogens through the lower atmosphere where they are implicated in ozone destruction and Hg^0 oxidation [*Simpson, et al.,* 2007 and references therein]. Stronger continental winds transported background O_3 and Hg^0 to the study site caused the concentrations to return to normal (non-AMDE) levels.

AMDE conditions are better identified in this study by using ozone mixing ratios rather than atmospheric TGM concentrations. Reactive gaseous and particulate Hg species can episodically reach or exceed 1 ng/m^3 during AMDEs [*Kirk, et al.,* 2006; *Lindberg, et al.,* 2002] and may occasionally compose a significant fraction of TGM. Furthermore, a strong correlation between ozone and Hg^0 between AMDE and non-AMDE periods throughout the polar springtime has been well documented [*Ebinghaus, et al.,* 2002; *Schroeder, et al.,* 1998; *Skov, et al.,* 2004; *Sprovieri, et al.,* 2005].

Exchange of Hg between air and surface snow

Surface snow collected from the upper 1 cm of the snowpack at both sampling sites contained elevated Hg levels during AMDE conditions (Figure 5). The Hg concentration is reported in pg Hg/g melted snow, so an increase in the Hg concentration

can be achieved by either gaining Hg or losing H_2O or both. Horizontal mixing of surface snow was negligible during AMDE conditions, so changes in $Hg_{surface}$ represent snow-atmosphere exchange of Hg and H_2O. High velocity winds prominent during non-AMDE conditions vigorously mobilized snow grains and broadened the Hg mass balance beyond atmospheric exchange. Therefore, $Hg_{surface}$ can be compared in a meaningful time-series of snow-atmosphere exchange during AMDE conditions but not normal conditions. Downward exchange of Hg with deeper, interstitial air during AMDE conditions is unlikely because of weak wind pumping.

Deposition of background TGM from the overlying vertical air column can account for the Hg gains to surface snow during the observed AMDE conditions. For example, atmospheric TGM levels dropped while Hg concentrations in surface snow at Site 1 increased from background levels of 4.1 to 15.5 pg/g to a concentration plateau of 180 to 240 pg/g within two days of the onset of AMDE conditions. Assuming a background TGM concentration of 1.6 ng/m^3 and a typical snow density of 0.3 g/cm^3, the observed Hg gain to the upper 1 cm of 0.16 to 0.21 ng can be explained by quantitative oxidation and deposition of TMG available in the vertical boundary layer to a height of between 150 to 450 m. In this scenario, the background TGM supply is completely transferred to the snow surface. In addition, weak AMDE winds prevent an influx of air containing higher TGM concentrations from regions not experiencing AMDE conditions. Our explanation is consistent with previous aircraft and sonde studies that constrained Hg depletion to an elevation of between 100 and 1000 m [*Lindberg, et al.,* 2002] and ozone and Hg depletion to a height of 300-400 m [*Tackett, et al.,* 2007 and references therein].

Gradual increases in $Hg_{surface}$ observed at Site 2 throughout the AMDE probably resulted from a different mechanism than at Site 1. The presence of a snow fence created turbulence and reduced wind speed, forming a snow drift at Site 2 that is less representative of the regional snowpack than Site 1. Surface hoar grew on the snow drift sampled at Site 2 and may have scavenged atmospheric Hg via a mechanism relating to unusual atmospheric turbulence and Hg^{2+} scavenging during vapor phase crystal growth. This mechanism may also be effect at pressure ridges. On 29 March, snow from both Site 2 and the pressure ridge contained approximately half the Hg concentration of snow at Site 1. Surface hoar is thought to be capable of scavenging high levels of Hg^{2+} when proximal to an Hg^{2+} source during its vapor phase condensation [*Douglas, et al.,* 2005]. However, surface hoar is a poor scavenger during low wind conditions [*Colbeck,* 1988], which may explain the gradual, rather than step-wise, $Hg_{surface}$ enhancement at Site 2 and the lower Hg concentrations of surface hoar at Site 2 and the pressure ridge with respect to Site 1.

The Hg concentration in snowfall was highest during non-AMDE conditions and probably results from scavenging of TGM by snow crystals in the air column. The Hg-depleted boundary layer during AMDE conditions therefore has little to no Hg available for scavenging by snowfall. The elevated $Hg_{snowfall}$ sample collected during the AMDE (363 pg/g, 25 March) could be explained by scavenging of recently emitted and re-oxidized Hg. After the return to non-AMDE conditions, one snowfall sample contained much less Hg than other non-AMDE samples (118 pg/g on 2 April) and was potentially diluted by a larger ice volume.

Nighttime Hg^{2+} deposition mechanism

The enhancement of Hg$_{surface}$ at Site 2 tended to occur overnight in the absence of photochemical reactions. Mercury deposition and re-emission occur simultaneously, but the balance shifted between net daytime Hg^0 emission and net nighttime Hg^{2+} deposition. Two additional lines of evidence support daytime Hg^0 emission from surface snow: (1) ambient atmospheric TGM values measured 5 cm above the snowpack surface peaked daily around solar noon, (2) and TGM emission patterns from field-based flux chamber experiments peaked during maximum solar intensity. Nighttime water loss is unlikely because decreasing surface temperature increases relative humidity and favors moisture deposition, rather than sublimation. Moisture deposition enhances the specific surface area of the snow surface by adding high surface area hoar frost crystals [*Domine, et al., 2005*]. During AMDE conditions, the growth and deposition of surface hoar crystals could enhance Hg scavenging at night. However, this mechanism cannot explain Hg$_{surface}$ gains at Site 1 where surface hoar frost was absent. We describe two plausible mechanisms of Hg gain to explain nighttime Hg$_{surface}$ enhancements.

First, a chemical (rather than photochemical) mechanism may generate atmospheric Hg^{2+} at night and enhance the mass ratio of Hg to water. We speculate that a chemical oxidation pathway similar to that proposed to explain observations at the South Pole [*Brown, et al.,* 2006] may be active during AMDEs. In this nocturnal mechanism, O$_3$ and NO$_x$ are destroyed by heterogeneous dinitrogen pentoxide (N$_2$O$_5$) hydrolysis when sulfate aerosols and NO$_x$ precursors are present. Sulfate aerosols are present in coastal Arctic locations due to sources such as sea-spray aerosols, marine dimethyl sulfide release and as Arctic Haze (see review by Law and Stohl, [2007]). Atmospheric

NO_x sources include photolysis of nitrate ions in snow and have been documented in Barrow [*Honrath and Jaffe*, 1992], Alert, Canada [*Beine, et al.*, 2002] and at the South Pole [*Davis, et al.*, 2004]. Operation of a nighttime chemical oxidation pathway during a time that lacks photochemical Hg reduction would cause Hg deposition to dominate air-snow exchange at night.

Second, a physical mechanism related to the settling velocity of snow crystals may explain the net nighttime Hg deposition observed at Site 2. Large snow crystals will have more rapid settling velocities and lower Hg to water mass ratios than fine snow crystals. The lag time between maximum Hg^0 oxidation and scavenging at mid-day and deposition of Hg-sorbed snow crystals will be a function of snow crystal size and density and may explain the observed diurnal trend in $Hg_{surface}$. We calculate the settling velocity of snow crystals during laminar (i.e. windless, Figure 3) AMDE conditions by Stoke's settling:

$$v_s = D^2 \, g \, (\rho_p - \rho_f)/(18\eta)$$

where D is the particle diameter, g is the gravitational constant, ρ_p is the snow particle density, ρ_f is the density of -20°C air (1.394 kg/m^3) and η is the fluid viscosity of air at -20°C (1.659 x 10^{-5} Pa s). Assuming a crystal density of typical snow to be 15 g/cm^3 [*Cabanes, et al.*, 2002] and a particle diameter range of 110 to 250 μm based on a weighted average of sector plate clusters, bullet clusters and snow grain columns dimensions reported by Walden and others, [2003], we estimate typical snow requires 0.6 to 2 hours to settle from a height of 150 to 450 m. Diamond dust is commonly termed "clear sky precipitation" and refers to very small ice crystals of plate, thick plate or column crystal habit that form by direct vapor deposition onto heterogeneous nucleation

sites [*Girard and Blanchet*, 2001; *Intrieri and Shupe*, 2004; *Ohtake, et al.*, 1982; *Schnell, et al.*, 1989; *Walden, et al.*, 2003]. If we assume a maximum diamond dust diameter of 30 μm [*Girard and Blanchet*, 2001; *Walden, et al.*, 2003] and a maximum density of 0.15 g/cm^3 [*Cabanes, et al.*, 2002; *Domine, et al.*, 2002], then we calculate a maximum settling rate of diamond dust from an elevation of 150 to 450 m to the ground surface to be 10 to 30 hours. The presence of any winds would enhance the settling velocity and shorten the settling time for both crystal types. Therefore, preferential settling of larger ice crystals and delayed settling of diamond dust presents a plausible (but speculative) mechanism for nighttime delivery of Hg-enriched ice crystals to the Arctic snowpack during AMDE conditions.

Net loading of Hg to the Arctic snowpack

We have documented rapid and significant increases in the Hg concentration of surface snow during AMDE conditions. It is of utmost importance to estimate how much AMDE-derived Hg remains in the seasonal snowpack and is thus available to be transferred to the Arctic ecosystem during snowmelt. The majority of snowfall forming the snowpack near Barrow fell prior to the AMDE season and contained low, background levels of Hg. Surface and core data during and after the AMDE demonstrate that Hg-enrichment was stratified with a high-Hg surface layer atop a low-Hg snow column. Concentrations of Hg in the surface snow decreased readily throughout the season and snowpack cores decreased in Hg concentration before snowmelt began in late May (Figure 7). Loss of Hg from the snowpack later in the season could result from physical transport and/or chemical reduction and emission of Hg^0 to the atmosphere. Our data

support neither the observation of dramatic Hg increases in Arctic snow with increasing light intensity nor net loading of Hg to the Arctic ecosystem by AMDE mechanisms. We used flux chambers to quantify Hg^0 emission from a subset of natural, Hg-enriched surface snow to explore Hg emission mechanisms and rates.

Flux chamber experiments

Field-based flux chamber experiments more closely resemble natural processes than laboratory experiments because they can utilize fresh, unmetamorphosed snow and are exposed to the ambient atmospheric conditions (e.g. chemical constituents, sunlight and temperature). However, field-based experiments do not allow a high level of control over experimental conditions and do not perfectly replicate conditions experienced by the natural snowpack. For example, flux chambers were filled with surface snow rather than a full-column sample representative of the entire snowpack, and this could potentially enhance total Hg content within the chamber. Nonetheless, important mechanistic information about Hg emission, such as whether the strong diurnal pattern of TGM emission was a result of temperature or light dependent reactions, can be gained from these experiments and is described below.

Maximum TGM emission occurred shortly after solar noon in every flux chamber experiment and TGM emission during hours of darkness was not detected (Figure 8). Data from the heated flux chamber experiment demonstrate that snow may emit more Hg^0 when sub-freezing temperatures are increased in the absence of sunlight. However, emission of 7 ng/m^3 TGM (data not shown) might alternately be explained by indirect photochemical reactions between photolabile reactants entering the chamber inlet and

chemically reducing Hg. Similar laboratory experiments found that alpine snow did not emit more TGM as the temperature rose from -12°C to -4°C in the absence of light [*Dommergue et al.,*, 2007]. Release of Hg^0 from snow by sub-freezing, temperature-induced mechanisms did not cause the diurnal TGM emission pattern observed in our experiments. Instead, the diurnal Hg emission patterns observed in the chamber experiments resulted directly from photochemical reactions.

While light intensity was the dominant control over the diurnal TGM release pattern, initial Hg concentration in snow had more control over the TGM emission rate than did light intensity (Figure 10). TGM emission rates were highly variable (note the different vertical scales in Figure 8) until normalized to the Hg content of the bulk chamber and of the surface area of exposed snow. Chambers consistently emitted 4 to 7% of their total Hg content within one day, 45% ± 0.03 of which occurred at mid-day between 12:30 and 15:30 (Table 2, "% of daily emission at mid-day"). If we assume photochemistry was active to a depth of 1 cm over the surface area of snow exposed at the surface and along three vertical chamber walls (0.47 m^2), 12-23% was emitted each day during AMDE conditions and 7% was emitted under non-AMDE conditions (Table 2; "% Hg emitted from exposed volume"). Emission of TGM from chamber snow was not measured on subsequent days, and it is conceivable that these data represent loss of readily reducible Hg and therefore maximum emission rates.

We tested the influence of UV radiation on TGM emission from natural snow (Figure 8; Exp 7) because UV_B has been shown to be influential in photoreducing Hg^{2+} in natural waters [*Poulain, et al.,* 2004]. TGM emission decreased by 25% when UV was fully attenuated through the chamber lid and at least 75% of incident UV was attenuated

through the vertical chambers walls (Figure 9). If only UV radiation can reduce Hg, then UV penetration through the vertical chamber walls over an area of 0.19 m^2 would have had to produce the observed TGM release. In this scenario, 28% of the Hg available in the exposed volume would have been emitted within one day. This emission fraction is four times larger than from any other experiment in this study and suggests that this scenario is inaccurate. Therefore, visible light and UV radiation are probably both important in the photoreduction of Hg in snow.
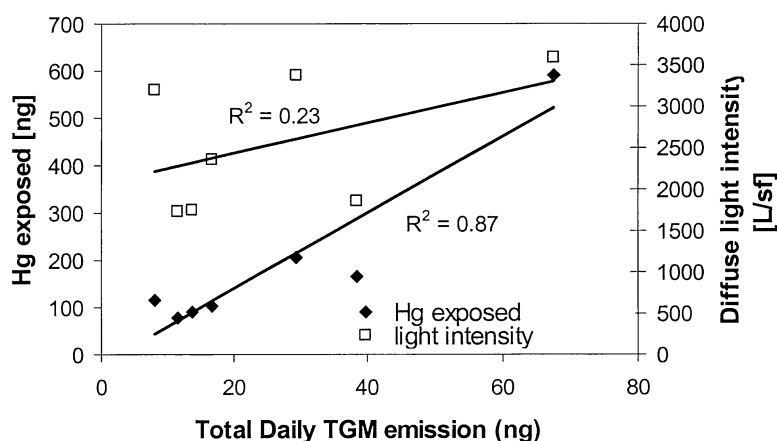
Figure 10: Total daily Hg emission versus both Hg content of exposed snow volume (1 cm depth on three chamber walls and upper snow surface, left vertical axis) and mid-day average diffuse light intensity (right vertical axis).

CONCLUSION

We observed large and rapid increases in the Hg concentration of surface snow during AMDE conditions, but very little change in the overall snowpack Hg content was observed. Low-speed, on-shore winds and stable boundary layer meteorology prevented physical mixing of the snowpack and resulted in deposition of Hg^{2+} to a thin, concentrated layer of surface snow. Therefore, the high Hg concentrations did not permeate deeply into the snow column. When AMDE conditions ended and strong continental winds returned, physical mixing diluted the Hg-enhanced surface layer with lower Hg concentration snow at depth. Snow-atmosphere exchange during non-AMDE conditions was dominated by photoreduction and emission of Hg^0. Field experiments typically lost 5% of their Hg content within one day. Photochemical processes continued throughout the spring and AMDE Hg-gains to the snow pack do not appear to have contributed Hg to the terrestrial or aquatic ecosystems during snowmelt. Future experiments should increase our understanding of how AMDE-derived Hg evades from snowpacks and test whether snow maintains the rate of Hg loss of 5% per day after long-term exposure to sunlight. In addition, physical and chemical mechanisms of Hg deposition during AMDEs need to be better understood in order to assess how potential changes in meteorological conditions due to climatic warming in the Arctic may affect atmospheric delivery of Hg to snow in the coastal Arctic.

REFERENCES

Ariya, P. A., A. P. Dastoor, M. Amyot, W. H. Schroeder, L. Barrie, K. Anlauf, F. Raofie, A. Ryzhkov, D. Davignon, J. Lalonde, and A. Steffen (2004), The Arctic: a sink for mercury, *Tellus Series B-Chemical And Physical Meteorology*, *56*, 397-403.

Barrie, L., and U. Platt (1997), Arctic tropospheric chemistry: an overview, *Tellus Series B-Chemical And Physical Meteorology*, *49*, 450-454.

Barrie, L. A., J. W. Bottenheim, R. C. Schnell, P. J. Crutzen, and R.A. Rasmussen (1988), Ozone Destruction And Photochemical-Reactions At Polar Sunrise In The Lower Arctic Atmosphere, *Nature*, *334*, 138-141.

Beine, H. J., R. E. Honrath, F. Domine, W. R. Simpson, and J.D. Fuentes (2002), NOx during background and ozone depletion periods at Alert: Fluxes above the snow surface, *Journal Of Geophysical Research-Atmospheres*, *107*, 4584, doi:10.1029/2002JD002082.

Berg, T., S. Sekkesaeter, E. Steinnes, A. K. Valdal, and G. Wibetoe (2003), Springtime depletion of mercury in the European Arctic as observed at Svalbard, *Science Of The Total Environment*, *304*, 43-51.

Brooks, S. B., A. Saiz-Lopez, H. Skov, S. E. Lindberg, J. M. C. Plane, and M. E. Goodsite (2006), The mass balance of mercury in the springtime arctic environment, *Geophysical Research Letters*, *33*, L13812, doi: 10.1029/2005GL025525.

Brown, S. S., T. B. Ryerson, A. G. Wollny, C. A. Brock, R. Peltier, A. P. Sullivan, R. J. Weber, W. P. Dube, M. Trainer, J. F. Meagher, F. C. Fehsenfeld, and A. R. Ravishankara (2006), Variability in nocturnal nitrogen oxide processing and its role in regional air quality, *Science*, *311*, 67-70. doi: 10.1126/science.1120120

Cabanes, A., L. Legagneux, and F. Domine (2002), Evolution of the specific surface area and of crystal morphology of Arctic fresh snow during the ALERT 2000 campaign, *Atmospheric Environment*, *36*, 2767-2777.

Colbeck, S. C. (1988), On The Micrometeorology Of Surface Hoar Growth On Snow In Mountainous Area, *Boundary-Layer Meteorology*, *44*, 1-12.

Davis, D., G. Chen, M. Buhr, J. Crawford, D. Lenschow, B. Lefer, R. Shetter, F. Eisele, L. Mauldin, and A Hogan (2004), South Pole NOx chemistry: an assessment of factors controlling variability and absolute levels, *Atmospheric Environment*, *38*, 5375-5388.

Domine, F., A. Cabanes, and L. Legagneux (2002), Structure, microphysics, and surface area of the Arctic snowpack near Alert during the ALERT 2000 campaign, *Atmospheric Environment*, *36*, 2753-2765.

Domine, F., A. S. Taillandier, W. R. Simpson, and K. Severin (2005), Specific surface area, density and microstructure of frost flowers, *Geophysical Research Letters*, *32* L13502, doi: 10.1029/2005GL023245.

Dommergue, A., C. P. Ferrari, P. A. Gauchard, C. F. Boutron, L. Poissant, M. Pilote, P. Jitaru, and F. C. Adams (2003), The fate of mercury species in a sub-arctic snowpack during snowmelt, *Geophysical Research Letters*, *30*, 1621, doi: 10.1029/2003GL017308.

Douglas, T., M. Sturm, W. Simpson, J. Blum, L. Alvarez-Aviles, G. Keeler, D. Perovich, A. Biswas and K. Johnson (*in press*), The influence of snow and ice crystal formation and accumulation on mercury deposition to the Arctic., *Environmental Science & Technology*.

Douglas, T. A., M. Sturm, W. R. Simpson, S. Brooks, S. E. Lindberg, and D. K. Perovich (2005), Elevated mercury measured in snow and frost flowers near Arctic sea ice leads, *Geophysical Research Letters*, *32*, L04502, doi: 10.1029/2004GL022132.

Ebinghaus, R., H. H. Kock, C. Temme, J. W. Einax, A. G. Lowe, A. Richter, J. P Burrows, and W. H. Schroeder (2002), Antarctic springtime depletion of atmospheric mercury, *Environmental Science & Technology*, *36*, 1238-1244.

Ferrari, C. P., P. A. Gauchard, K. Aspmo, A. Dommergue, O. Magand, E. Bahlmann, S. Nagorski, C. Temme, R.
Ebinghaus, A. Steffen, C. Banic, T. Berg, F. Planchon, C. Barbante, P. Cescon, and C. F. Boutron (2005), Snow-to-air exchanges of mercury in an Arctic seasonal snow pack in Ny-Alesund, Svalbard, *Atmospheric Environment*, *39*, 7633-7645.

Fitzgerald, W. F., and C. H. Lamborg (2003), Geochemistry of Mercury in the Environment, *Treatise on Geochemistry*, *9*, 107-148.

Gauchard, P. A., K. Aspmo, C. Temme, A. Steffen, C. Ferrari, T. Berg, J. Strom, L. Kaleschke, A. Dommergue, E. Bahlmann, O. Magand, F. Planchon, R. Ebinghaus, C. Banic, S. Nagorski, P. Baussand, and C. Boutron (2005), Study of the origin of atmospheric mercury depletion events recorded in Ny-Alesund, Svalbard, spring 2003, *Atmospheric Environment*, *39*, 7620-7632.

Girard, E., and J. P. Blanchet (2001), Microphysical parameterization of arctic diamond dust, ice fog, and thin stratus for climate models, *Journal Of The Atmospheric Sciences*, *58*, 1181-1198.

Honrath, R. E., and D. A. Jaffe (1992), The Seasonal Cycle Of Nitrogen-Oxides In The Arctic Troposphere At Barrow, Alaska, *Journal Of Geophysical Research-Atmospheres*, *97*, 20615-20630.

Intrieri, J. M., and M. D. Shupe (2004), Characteristics and radiative effects of diamond dust over the western Arctic Ocean region, *Journal Of Climate*, *17*, 2953-2960.

Kirk, J. L., V. L. S. Louis, and M. J. Sharp (2006), Rapid reduction and reemission of mercury deposited into snowpacks during atmospheric mercury depletion events at Churchill, Manitoba, Canada, *Environmental Science & Technology*, *40*, 7590-7596.

Landis, M. S., M. Lynam, and R. K. Stevens (2005), *The measurement and source characterization of speciated atmospheric mercury*, Kluwer Ltd.

Landis, M. S., R. K. Stevens, F. Schaedlich, and E. M. Prestbo (2002), Development and characterization of an annular denuder methodology for the measurement of divalent inorganic reactive gaseous mercury in ambient air, *Environmental Science & Technology*, *36*, 3000-3009.

Law, K. S., and A. Stohl (2007), Arctic air pollution: Origins and impacts, *Science*, *315*, 1537-1540, doi: 10.1126/science.1137695.

Lindberg, S. E., S. Brooks, C-J Lin, K. Scott, T. Meyers, L. Chambers, M. Landis, and R. Stevens (2001), Formation of reactive gaseous mercury in the Arctic: evidence of oxidation of Hg° to gas-phase Hg-II compounds after Arctic Sunrise, *Water, Air, and Soil Pollution: Focus*, *1*, 295-302.

Lindberg, S. E., S. Brooks, C. J. Lin, K. J. Scott, M. S. Landis, R. K. Stevens, M. Goodsite, and A. Richter (2002), Dynamic oxidation of gaseous mercury in the Arctic troposphere at polar sunrise, *Environmental Science & Technology*, *36*, 1245-1256.

Lu, J. Y., W. H. Schroeder, L. A. Barrie, A. Steffen, H. E. Welch, K. Martin, L. Lockhart, R. V. Hunt, G. Boila, and A. Richter (2001), Magnification of atmospheric mercury deposition to polar regions in

springtime: the link to tropospheric ozone depletion chemistry, *Geophysical Research Letters*, *28*, 3219-3222.

Macdonald, R. W., T. Harner, and J. Fyfe (2005), Recent climate change in the Arctic and its impact on contaminant pathways and interpretation of temporal trend data, *Science Of The Total Environment*, *342*, 5-86.

Magos, L., and T. W. Clarkson (2006), Overview of the clinical toxicity of mercury, *Annals Of Clinical Biochemistry*, *43*, 257-268.

Ohtake, T., K. Jayaweera, and K. I. Sakurai, (1982), Observation Of Ice Crystal-Formation In Lower Arctic Atmosphere, *Journal Of The Atmospheric Sciences*, *39*, 2898-2904.

Oltmans, S. J., and W. D. Komhyr (1986), Surface Ozone Distributions And Variations From 1973-1984 Measurements At The Noaa Geophysical Monitoring For Climatic-Change Base-Line Observatories, *Journal Of Geophysical Research-Atmospheres*, *91*, 5229-5236.

Pomeroy, J. W., and D. M. Gray (1990), Saltation Of Snow, *Water Resources Research*, *26*, 1583-1594.

Poulain, A. J., J. D. Lalonde, M. Amyot, J. A. Shead, F. Raofie, and P. A. Ariya (2004), Redox transformations of mercury in an Arctic snowpack at springtime, *Atmospheric Environment*, *38*, 6763-6774.

Schnell, R. C., R. G. Barry, M. W. Miles, E. L. Andreas, L. F. Radke, C. A. Brock, M. P. McCormick, and J. L. Moore (1989), Lidar Detection Of Leads In Arctic Sea Ice, *Nature*, *339*, 530-532.

Schroeder, W. H., K. G. Anlauf, L. A. Barrie, J. Y. Lu, A. Steffen, D. R. Schneeberger, and T. Berg (1998), Arctic springtime depletion of mercury, *Nature*, *394*, 331-332.

Scott, K. J. (2001), Bioavailable mercury in arctic snow determined by a light-emitting mer-lux bioreporter, *Arctic*, *54*, 92-95.

Simpson, W. R., L. Alvarez-Aviles, T. A. Douglas, M. Sturm, and F. Domine (2005), Halogens in the coastal snow pack near Barrow, Alaska: Evidence for active bromine air-snow chemistry during springtime, *Geophysical Research Letters*, *32*, L04811, doi: 10.1029/2004GL021748.

Simpson, W. R., D. Carlson, G. Honninger, T. A. Douglas, M. Sturm, D. Perovich, and U. Platt (2007), First-year sea-ice contact predicts bromine monoxide (BrO) levels at Barrow, Alaska better than potential frost flower contact, *Atmospheric Chemistry And Physics*, *7*, 621-627.

Skov, H., J. H. Christensen, M. E. Goodsite, N. Z. Heidam, B. Jensen, P. Wahlin, and G. Geernaert (2004), Fate of elemental mercury in the arctic during atmospheric mercury depletion episodes and the load of atmospheric mercury to the arctic, *Environmental Science & Technology*, *38*, 2373-2382.

Slemr, F., E. G. Brunke, R. Ebinghaus, C. Temme, J. Munthe, I. Wangberg, W. Schroeder, A. Steffen, and T. Berg (2003), Worldwide trend of atmospheric mercury since 1977, *Geophysical Research Letters*, *30*, 1516, doi: 10.1029/2003GL016954.

Slemr, F., G. Schuster, and W. Seiler (1985), Distribution, Speciation, And Budget Of Atmospheric Mercury, *Journal Of Atmospheric Chemistry*, *3*, 407-434.

Sprovieri, F., N. Pirrone, M. S. Landis, and R. K. Stevens (2005), Oxidation of gaseous elemental mercury to gaseous divalent mercury during 2003 polar sunrise at Ny-Alesund, *Environmental Science & Technology*, *39*, 9156-9165.

Steffen, A., T. A. Douglas, M. Amyot, P. A. Ariya, K. Aspmo, T. Berg, J. Bottenheim, S. Brooks, F. Cobbett, A. P. Dastoor, A. Dommergue, R. Ebinghaus, C. Ferrari, K. Gardfeldt, M. Goodsite, D. Lean, A. J. Poulain, C. Scherz, H. Skov, J. Sommar, and C. Temme (2007), A synthesis of atmospheric mercury depletion event chemistry linking atmosphere, snow and water, *Atmospheric Chemistry And Physics Discussions*, *7*, 10837-10931.

Steffen, A., W. Schroeder, R. Macdonald, L. Poissant, and A. Konoplev (2005), Mercury in the Arctic atmosphere: An analysis of eight years of measurements of GEM at Alert (Canada) and a comparison with observations at Amderma (Russia) and Kuujjuarapik (Canada), *Science Of The Total Environment*, *342*, 185-198.

Steffen, A., W. H. Schroeder, G. Edwards, and C. Banic (2003), Mercury throughout polar sunrise 2002, *Journal De Physique Iv*, *107*, 1267-1270.

Sturm, M., and G. E. Liston (2003), The snow cover on lakes of the Arctic Coastal Plain of Alaska, USA, *Journal Of Glaciology*, *49*, 370-380.

Tackett, P. J., A. E. Cavender, A. D. Keil, P. B. Shepson, J. W. Bottenheim, S. Morin, J. Deary, A. Steffen, and C. Doerge (2007), A study of the vertical scale of halogen chemistry in the Arctic troposphere during Polar Sunrise at Barrow, Alaska, *Journal Of Geophysical Research-Atmospheres*, *112*, D07306, doi: 10.1029/2006JD007785.

Walden, V. P., S. G. Warren, and E. Tuttle (2003), Atmospheric ice crystals over the Antarctic Plateau in winter, *Journal Of Applied Meteorology*, *42*, 1391-1405.

Wheatley, B., and S. Paradis (1995), Exposure Of Canadian Aboriginal Peoples To Methylmercury, *Water Air And Soil Pollution*, *80*, 3-11.